Electronic Supplementary Material (ESI) for Journal of Materials Chemistry B

Supporting Information

of

Molecular structure matters: PEG-b-PLA nanoparticles with hydrophilicity and deformability demonstrate their advantages for high-performance delivery of anti-cancer drugs

Zhanguo Yue[a,b,1], Zuoxiang You[a,c,1], Qinzheng Yang[c], Piping Lv[a,b], Hua Yue[a], Bin Wang[a], Dezhi Ni[a,b], Zhiguo Su[a], Wei Wei[a,*], and Guanghui Ma[a,*]

[a] *National Key Laboratory of Biochemical Engineering, Institute of Process Engineering, Chinese Academy of Sciences, Beijing, 100190, PR China Tel./fax: +86 10 82627072; E-mail: weiwei@home.ipe.ac.cn (W. Wei), ghma@home.ipe.ac.cn (G. Ma)*

[b] *University of Chinese Academy of Sciences, Beijing, 100049, PR China*

[c] *Department of Food and Bioengineering, Shandong Polytechnic University, Jinan, 250353, Shandong Province, PR China*

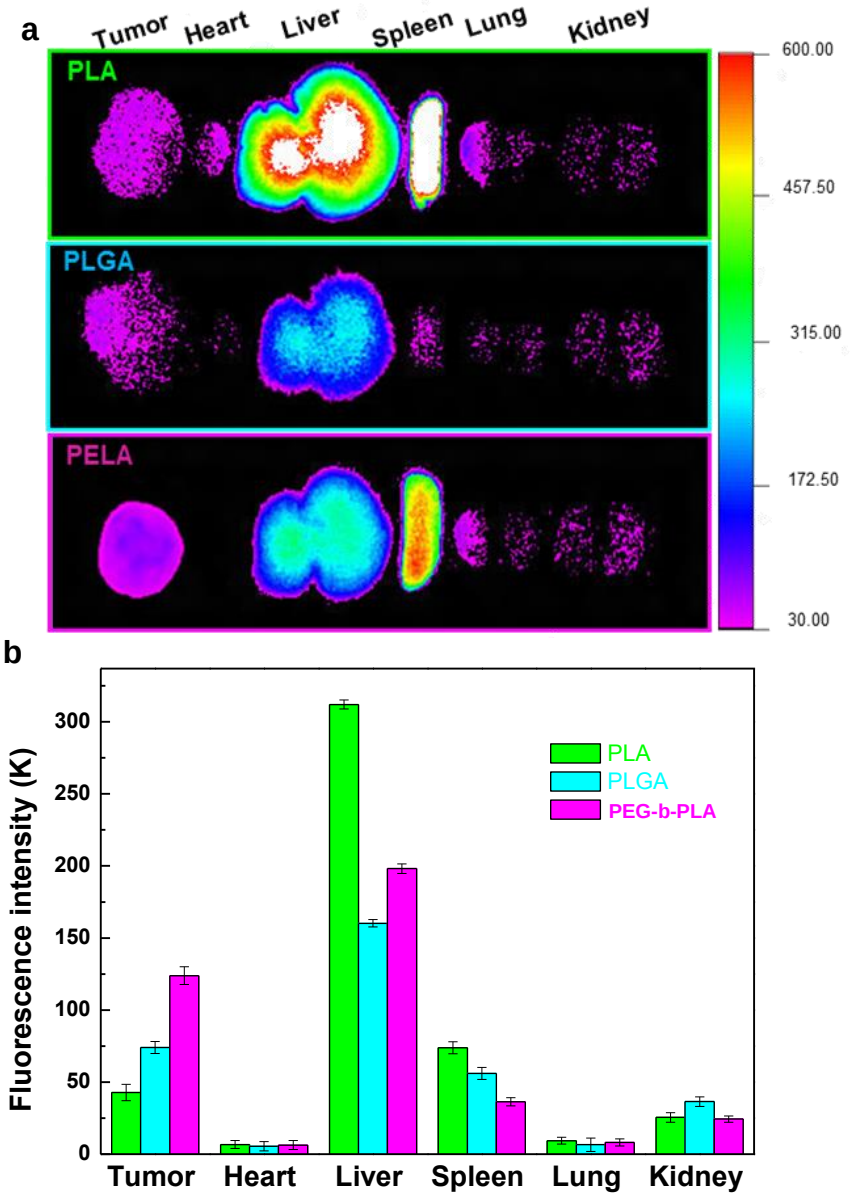

Figure S1. Biodistribution of PLA, PLGA, and PEG-b-PLA NPs after intravenous injection. (a) NIRF imaging of resected organs from LLC tumor-bearing C57BL/6 mice at 12 h post intravenous injection of NPs. (b) The corresponding fluoresce single intensity of resected organs. Data represent averages ± SD (n = 6).

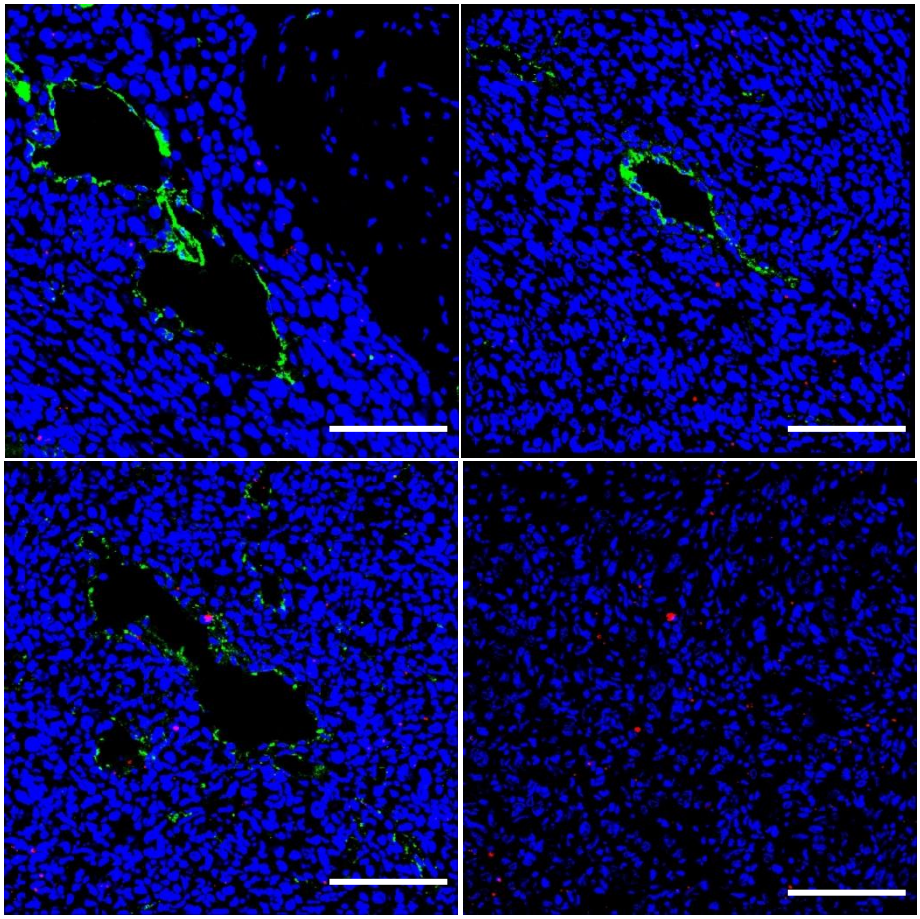

Figure S2. CLSM images of the frozen tumor tissue section showed the intratumoural location of PEG-b-PLA NPs 12 h after injection. Red, Cy5-labled NPs; green, rat anti-mouse CD31 mAb (FITC conjugate); blue, nuclei staining with Hoechst. Scale bars: 100 μm.

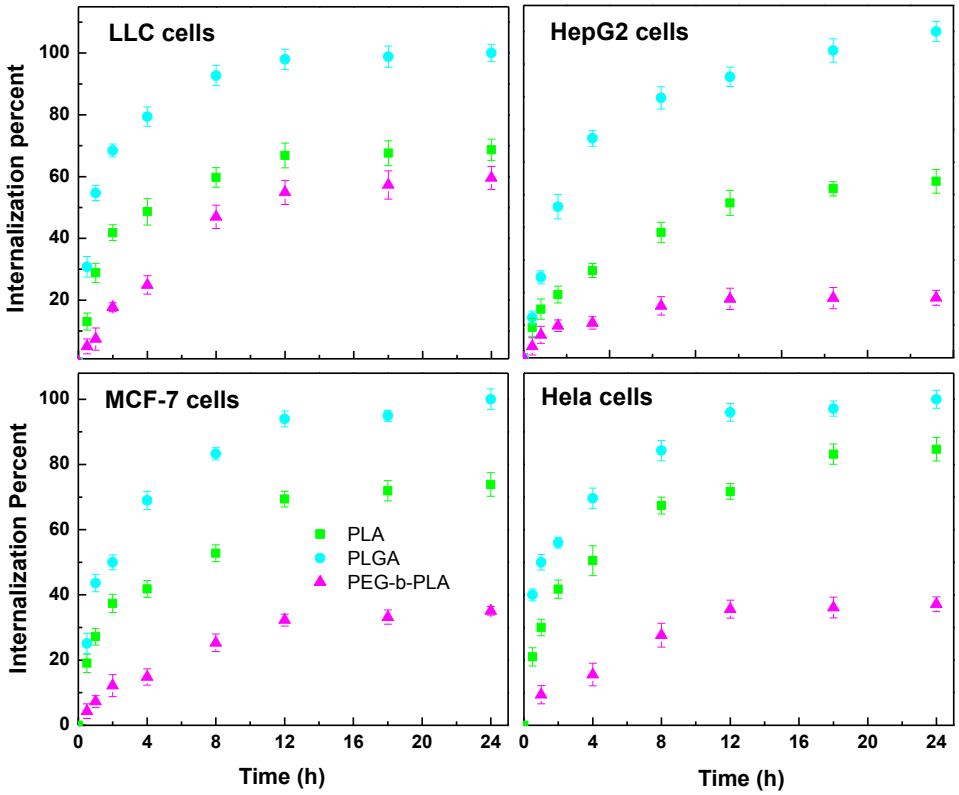

Figure S3.Cellular internalization kinetics of PLA, PLGA, and PEG-b-PLA NPs by four carcinoma cell lines. Cells cultured in 24-well plate were incubated with Cy5-labled NPs (100 μg/mL) for a desired period of time. Then, they were extensively washed by phosphate-buffered solution (PBS) for three times and analyzed on a CyAn ADP nine-color flow cytometer (Dako, Denmark). Data were acquired from 15 000 cells per sample. LLC, Lewis lung carcinoma; HepG2, human hepatocellular carcinoma cells; MCF-7, human breast adenocarcinoma cells; HeLa, human cervical carcinoma cells. Data represent averages ± SD (n = 3).

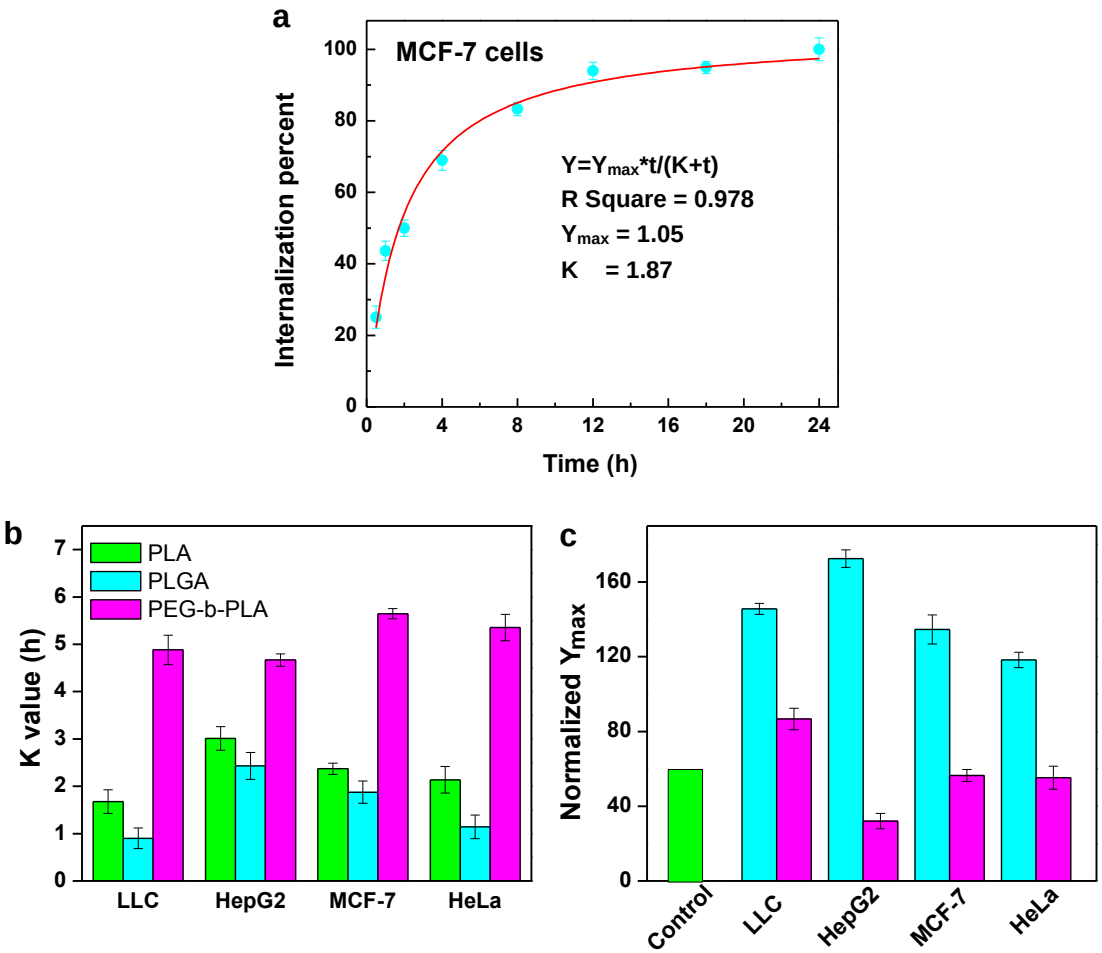

Figure S4. Mathematical analysis of cellular internalization patterns. The kinetics was well fitted to the Michaelis-Menten equation, taking PLGA uptake by MCF-7 cells as example (a). In this equation, Y_{max} is the maximal uptake level representing the saturated plateau value of the kinetic curves, and k is a rate constant. A smaller k reflects a quicker cellular internalization. After fitting, Uptake rate constant K value (b) and the maximum uptake amount Y_{max} value (c) of three NPs in different carcinoma cells could be obtained. The Y_{max} values of PLGA and PEG-b-PLA NPs in each cell line were normalized to their PLA counterparts.

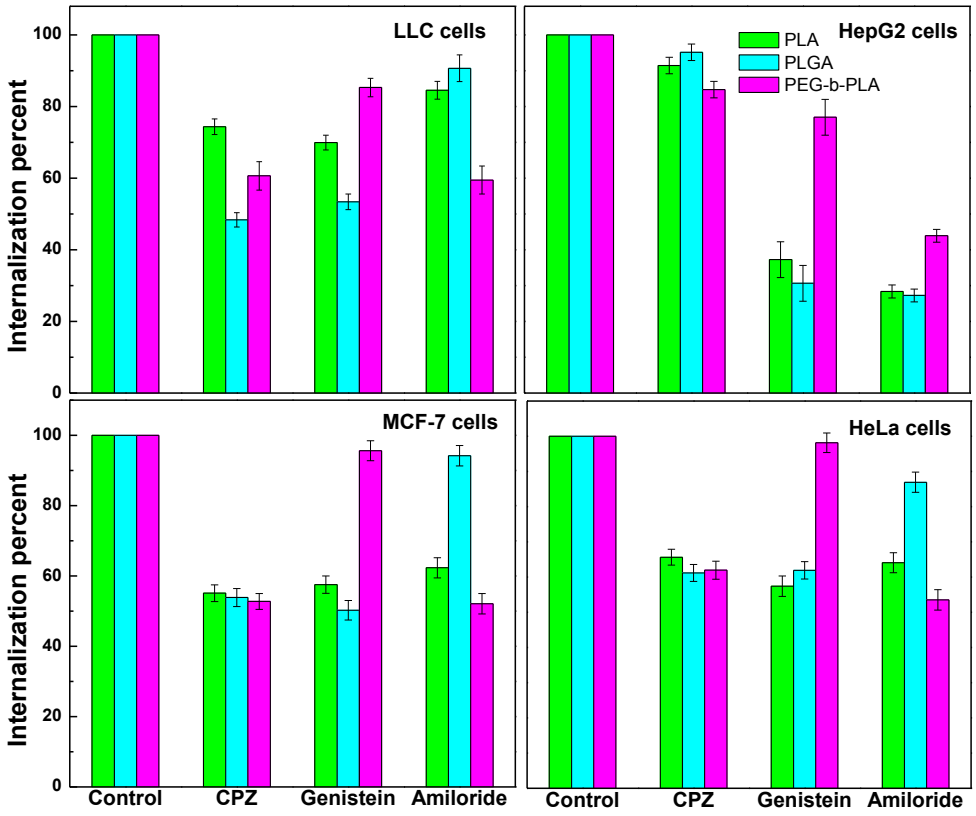

Figure S5. Evaluation on cellular uptake pathways of three NPs. For non-macrophage cells, the internalization pathways are usually divided into clathrin-mediated endocytosis, caveolae-mediated endocytosis, and macropinocytosis, which could be specifically inhibited by CPZ (30 μM), genistein (200 μM), and amiloride (100 μM), respectively. Data represent averages ± SD (n = 3).

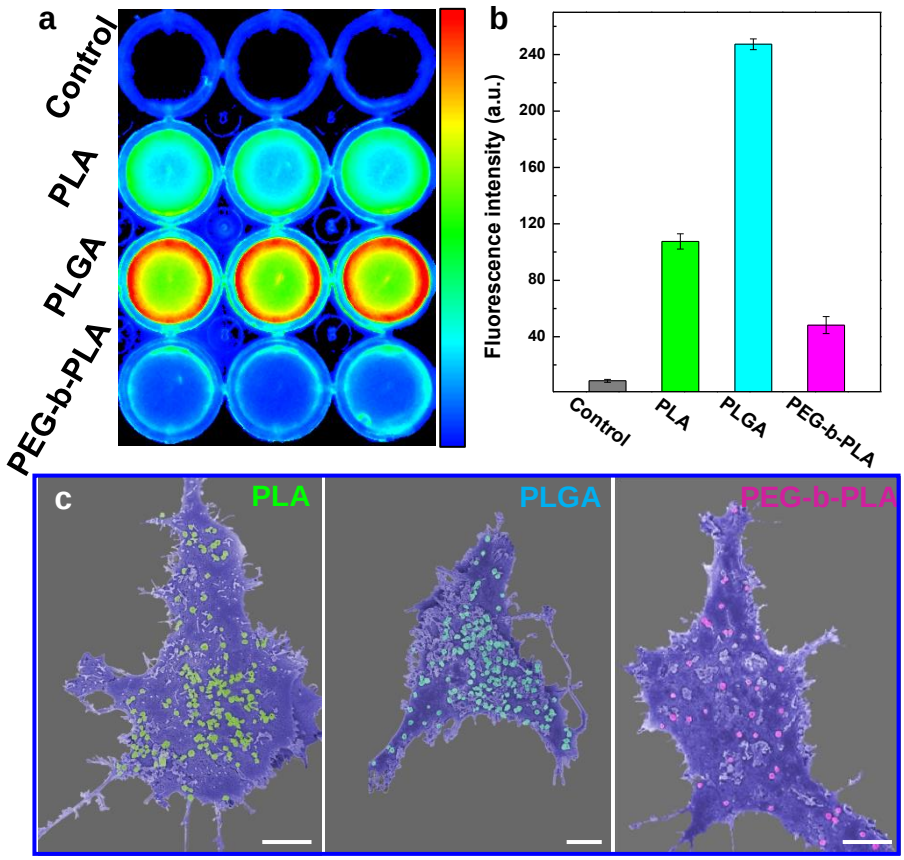

Figure S6. The bioadhesion of NPs on LLC cell surface 2 h after co-incubation at 4 ^{o}C. In-vivo Imaging System showing the fluorescence intensity of LLC cells and NP-adhered cells (a), with the corresponding quantitative diagram (b). (c) SEM images of LLC cells adsorbing with NPs. Data represent averages ± SD (n = 3). Scale bars: 5 μm.

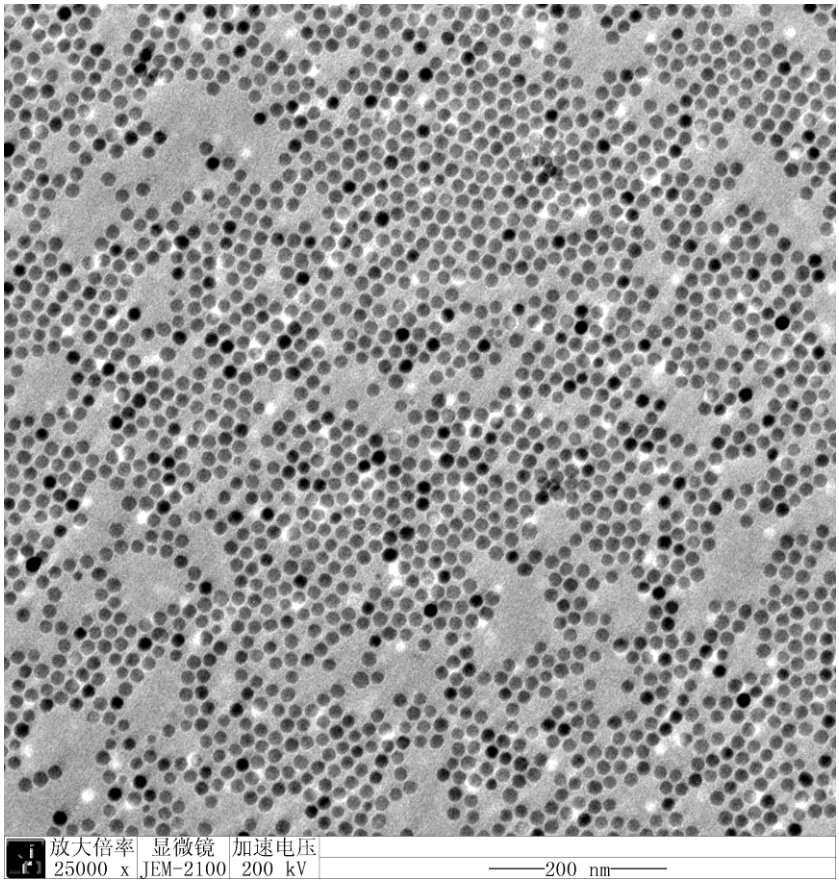

Figure S7. TEM image of Fe_3O_4 nanoparticles acquired from a JEOL JEM-2100F at 200 KV.

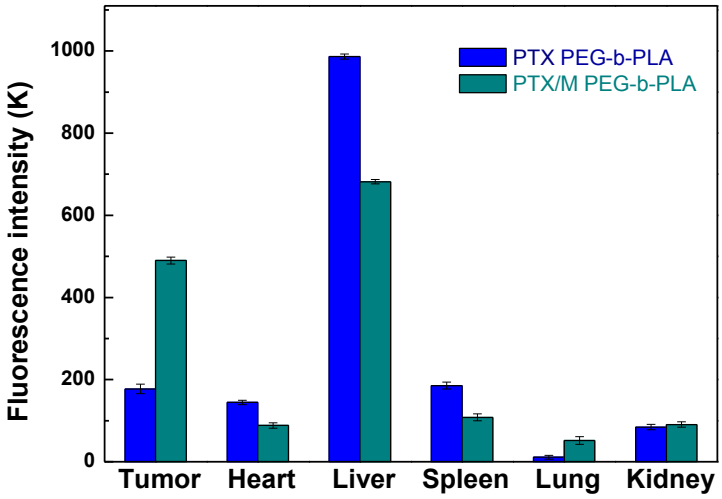

Figure S8. Biodistribution of PTX after intravenous injection of PTX PEG-b-PLA NPs and PTX/M PEG-b-PLA NPs.